Characterization of 2D boron nitride nanosheets with hysteresis effect in the Schottky junctions

NANO EXPRESS

OPEN ACCESS

RECEIVED
4 November 2020

REVISED
17 January 2021

ACCEPTED FOR PUBLICATION
25 January 2021

PUBLISHED
10 February 2021

PAPER

Characterization of 2D boron nitride nanosheets with hysteresis effect in the Schottky junctions

Wilber Ortiz[1,*], **Nereida J Ramirez**[2], **Danilo Barrionuevo**[3], **Mohan K Bhattarai**[1] and **Peter Feng**[1,*]

[1] Department of Physics, University of Puerto Rico, San Juan, 00931, United States of America
[2] Department of Harvard-MIT Health Sciences and Technology, Harvard Medical School, Boston, MA 02446, United States of America
[3] Department of Mathematics and Physics, University of Puerto Rico, Cayey, PR, 00736, United States of America
[*] Authors to whom any correspondence should be addressed.

E-mail: wilber.ortiz1@upr.edu **and** peter.feng@upr.edu

Keywords: 2D boron nitride nanosheets, Schottky contacts, hysteretic characteristics

Abstract

Carbon doped two-dimensional (2D) hexagonal boron nitride nanosheets (BNNSs) are obtained through a CO_2—pulsed laser deposition (CO_2—PLD) technique on silicon dioxide (SiO_2) or molybdenum (Mo) substrates, showing - stable hysteresis characteristics over a wide range of temperatures, which makes them a promising candidate for materials based on non-volatile memory devices. This innovative material with electronic properties of n-type characterized in the form of back-to-back Schottky diodes appears to have special features that can enhance the device performance and data retention due to its functional properties, thermal-mechanical stability, and its relation with resistive switching phenomena. It can also be used to eliminate sneak current in resistive random-access memory devices in a crossbar array. In this sense constitutes a good alternative to design two series of resistance-switching Schottky barrier models in the gold/BNNS/gold and gold/BNNS/molybdenum structures; thus, symmetrical and non-symmetrical characteristics are shown at low and high bias voltages as indicated by the electrical current-voltage (I–V) curves. On the one hand, the charge recombination caused by thermionic emission does not significantly change the rectification characteristics of the diode, only its hysteresis properties change due to the increase in external voltage in the Schottky junctions. The addition of carbon to BNNSs creates boron vacancies that exhibit partially ionic character, which also helps to enhance its electrical properties at the metal-BNNS-metal interface.

1. Introduction

2D hexagonal boron nitride nanosheet (BNNS) exhibits a honeycomb structure analog of graphene. The spacing between 2-layers is about 0.332 nm, and the lattice distance between the B–B or N–N atom separations is 0.22 nm. It shows a strong (002) diffraction peak in the XRD spectrum [1, 2]. Moreover, BNNS presents a good thermal conductivity and stability over a wide range of temperatures.

BNNS bandwidth is in the range of 4–6 eV, by doping with enough carbon (C) [3, 4], the bandgap is minimized, and a set of discrete energy levels are formed in the gap of BNNS. Previous research has already shown that the electronic and electrical structures could be improved with the C content [5–8]. Furthermore, BNNS film appears to have stable features even at high temperatures, so it has a variety of applications in polymeric [9, 10], flexible electronics [11, 12], Junction Field Effect Transistor (JFET) [13, 14], magneto-optics [15], and optoelectronics based on 2D crystals [16], etc.

Based on the special properties of the BNNS film, we propose two models of back-to-back Schottky diodes with specific characteristics. First is an Au/BNNS/Au type model grown onto the Si/SiO_2 substrates [17]. The second is Au/BNNS/Mo, where BNNS is deposited directly on the molybdenum substrate.

In the I–V representation, Au/BNNS/Au-based rectifiers exhibit symmetric characteristics, while Au/BNNS/Mo is asymmetric. When measured under low bias voltage, both have their hysteresis switching

characteristics. These are consistent with the analysis of the Poisson equation in the metal/semiconductor interface (n-type material) [18, 19]. This behavior of the 2D material offers a way to achieve a high hysterical switching quality in both the 'set' and 'reset' states at low power consumption, which may propose an improvement to recent studies carried out on memory devices with a thinner BNO_x layer [20], as well as in the Ni/n-type 4H-SiC Schottky structure [21, 22]. For example, BN monolayer-based resistance nonvolatile studied under different electrodes that shown stable bipolar and unipolar nonvolatile switching was studied [23–25]. In the same manner, in a multilayer structure, it is possible to grow the thickness of the h-BN film, which enhances the charge capture center to achieve better Poole-Frenkel conduction [26–28], comparable to the Schottky effect. This behavior of BNNS shows promise for several applications, such as non-volatile memory devices [29], pulse voltages, etc In previous studies, hysteresis has only been tested in 2D materials with graphene oxide and molybdenum disulfide [30–32]. Although these showed charge traps in the oxide dielectric layer, these observations were limited to higher room temperature, so the BNNS film may be an ideal candidate to obtain a more stable hysteresis over a wide temperature range [33].

During the last several years, great progress has been made on investigations of resistance switching and electrical hysteresis. This is partially attributed to newly developed nanotechnologies that were used to effectively control material nanostructures and MEMS (Micro-Electro-Mechanical Systems) fabrication [34, 35]. The BNNS samples used in the present work are very different from previous work where a single atomic or multi-layer sheet was used. The present sample consists of a large number of super-thin BN nanosheets randomly distributed over the entire surface of the substrate [36, 37]. Fabrication is extremely simple and MEMS techniques are not necessary.

2. Experimental

2.1. Synthesis

A CO_2-pulsed laser-produced plasma deposition (CO_2 - PLD) technique with a laser wavelength of 10.6 μm and an output power of 75 W was used. Pulsed laser beam irradiates hexagonal Boron Nitride (h-BN) target at 200 mTorr pressure of CH_4 environment in a vacuum chamber. The distance (d) between the target and the substrate (Si/SiO_2 or Mo) could be adjusted to control the BNNS film growth rate, and in the present case, $d = 3$ cm was selected. The laser incident angle with respect to the target plane was 45° and a power density was 2×10^8 W cm^{-2} per pulse. The pulse repetition frequency was 5 Hz. The deposition was kept at 300 °C for 20 min until thin films were achieved. A detailed description of the technical operation of CO_2—PLD can be found in reference [38].

The advantage of using PLD is to reduce the sheets' stress to yield large, highly flat, high-quality BNNSs. In contrast, traditional chemical synthesis often contains multi-component substance rather than a pure element. Furthermore, high temperatures in chemical synthesis such as CVD (Chemical Vapor Deposition) would not only vaporize impurities inside the chamber but also result in internal stresses that may affect the crystalline structures of the 2D sheets.

As we mentioned, the present samples consist of a large number of super-thin BN nanosheets randomly distributed over the entire surface of the substrate. Fabrication is very simple and MEMS techniques are not necessary.

2.2. Set-up

Two back-to-back Schottky barrier structures were fabricated in the present study to obtain different electrical properties. First were performed with Au/BNNS/Au junctions, as shown in figure 1(a). According to the synthesis method, BNNSs were deposited onto the Si/SiO_2 substrates. Then, the gold electrode elements were deposited in an argon gas environment at a power level of 250 watts by a sputtering method. The sputtering rate was 10 seconds to produce the gold film of 80 nm on 1 μm thick BNNS film where the typical thickness of single sheet is around 3–4 nm. The separation between the gold electrodes was 1 mm to form the back-to-back Schottky diode. In the same way, for Au/BNNS/Mo junctions, BNNSs were grown on the Mo substrate using the same techniques as the first case, as shown in figure 2(b). Each of the Schottky diodes was connected to an external power supply whose voltage variable (V) was 0 to 20 V, and fixed resistance (R_0) was 10 MΩ. Then, a heater was used to change the operating conditions of the Schottky structure on the I–V curve in the range of 0 to 170 °C.

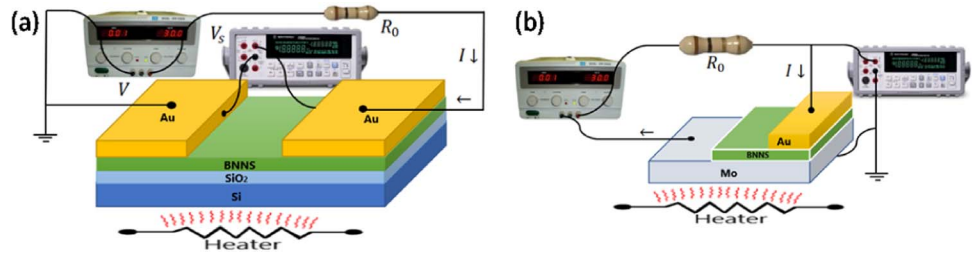

Figure 1. Schematic representation of the I–V measurements setup in Au/BNNS/Au and Au/BNNS/Mo contacts. (a) and (b) illustrate the Schottky contacts deposited on Si/SiO_2 and Mo substrates. Au and Mo are solid conductors while the BNNS film is a two-dimensional crystalline form of the h-BN.

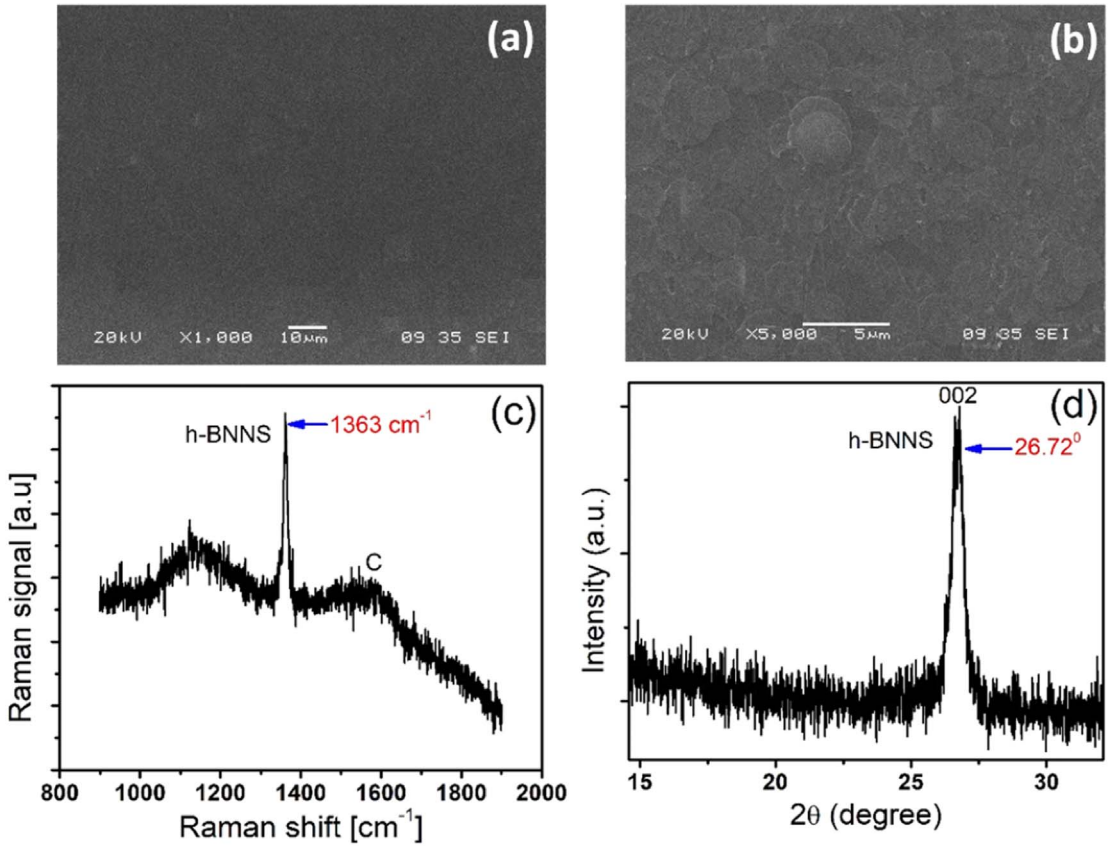

Figure 2. The structure of the BNNS film shown through (a)–(b) scanning electron microscopy (SEM) on the 10 um, 5 μm scale bar, (c) Raman scattering spectrum, (d) and x-ray diffraction.

3. Results and discussion

3.1. BNNS structure characterizations

SEM image of the BNNS film indicated that the obtained sample has a uniform and compact surface of round-shaped layers at the 10 μm scale, as shown in figure 2(a). Following an increase at the 5 μm scale, several small sheets were exhibited, which is characteristic of multilayer films as shown in figure 2(b). Instead, the Raman spectrum of the BNNS exhibits the peak around 1350 to 1360 cm^{-1} belonging to the Raman active vibrational mode (E_{2g}) [39, 40], as shown in figure 2(c), which is compatible with measurements analogous to these and is directly related to a hexagonal phase of BNNS.

X-ray diffraction (XRD) about BNNS film has a highly crystalline structure with the most intense and sharp peak at $2\theta = 26.77°$, corresponding to the crystallographic plane (002), as shown in figure 2(d) [41]. Using Bragg's law, we calculated the interlayer distance at BNNS film through relation

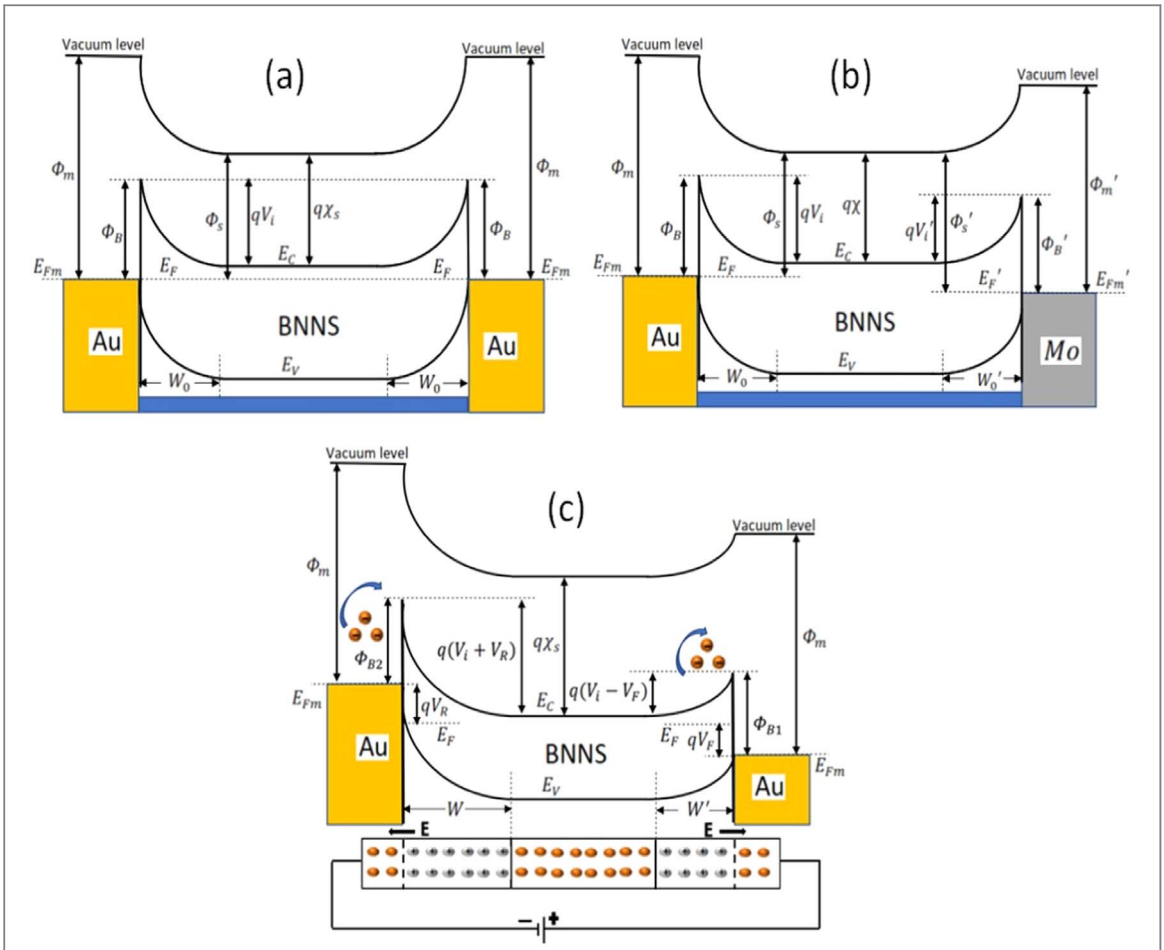

Figure 3. Back-back Schottky barrier formed at metal-semiconductor-metal junctions. (a)–(b) Energy band diagrams of metal and semiconductor (n-type) after contacts, (c) energy band diagrams with external bias voltage.

$$d = \frac{n\lambda}{2\sin\theta}, \tag{1}$$

where d is the interlayer distance of the crystalline plane measured in nm, λ is the wavelength of the x-ray source ($\lambda = 1.54$ Å), n is the order of reflection ($n = 1$), and θ is the angle of incidence in degrees of the plane. In fact, if analyzing the crystalline plane (002), the interlayer distance is 0.332 nm, which is within the range of the values established previously [42].

Very detailed descriptions of measurements of sheet thicknesses can be found in our previous work [43, 44]. A high-resolution TEM (Transmission Electron Microscope) was used to estimate the thickness of the single sheet by measuring the fringe pattern at the sheet's edge. Each fringe is related to a single atomic layer with a thickness around 0.33 nm. Accordingly, the thickness of the obtained BNNS can be estimated around 3–4 nm (8–11 layers).

3.2. Energy band diagram of back-to-back Schottky barriers

In this section, we propose a model based on energy band theory for the special case of two back-to-back Schottky diodes with two identical (Au-Au) and different contacts (Au-Mo). First, in the equilibrium state, Au/BNNS/Au contacts are a symmetric Schottky structure under the same vacuum level, as shown in figure 3(a). Alignment of Fermi energy leads to the formation of band diagrams and the barrier height in the metal/semiconductor interface states. These junctions produce different energy values in the Schottky barrier, where Φ_m is the work function of the gold (5.2 eV), Φ_s is the work function of the semiconductor, Φ_B is the barrier height ($\Phi_B = \Phi_m - q\chi_s$), $q\chi_s$ is the electron affinity of the semiconductor (the electron affinities of Au and Mo are 222.8 kJ mol^{-1} and 71.9 kJ mol^{-1}), E_{Fm} is the Fermi level of the gold (5.20 eV), E_F is the Fermi level of the semiconductor, E_V is the valence band edge, E_C is the conduction band edge, V_i is the built-in-voltage barrier ($qV_i = \Phi_m - \Phi_s = \Phi_B - (E_c - E_F)$), and W is the thickness of the depletion region, which depends on the concentration of ionized acceptor atoms. In contrast, Au/BNNS/Mo contacts have different barrier heights relative to the vacuum level in the equilibrium state, resulting in asymmetric structure, as shown in figure 3(b). Molybdenum band diagrams differ from gold at the metal/semiconductor interface, which is represented by

prime values; where $\Phi_m{}'$ is the work function of the molybdenum (4.6 eV), $E_F{}'$ is the Fermi level (4.20 eV), $\Phi_B{}'$ is the barrier height, etc.

Since the contact is metal and the semiconductor is n-type, the built-in-voltage barrier is expressed by

$$V_i = \frac{\Phi_B}{q} - \frac{kT}{q}\ln\left(\frac{N_C}{N_D}\right), \tag{2}$$

where q is the elementary charge, k is the Boltzmann constant, T is the absolute temperature, N_C is the effective state density in the conduction band that is constant for a given temperature, and N_D is the donor doping level. If we use moderate to lower doped semiconductors, we can reduce the Schottky barrier even further.

When an external voltage is applied to the back-to-back Schottky diodes, electron-hole pairs are generated, creating the charge flow and voltage drops on single diodes, as shown in figure 3(c). Electrons tend to move toward a positive bias because the voltage drop from V_i to $V_i - V_F$ on 2D semiconductor induces a narrow depletion region (W). On the contrary, under negative bias, the voltage drop increases from V_i to $V_i + V_R$, which in turn causes a wide depletion region. This behavior of the back-to-back Schottky diodes is directly related to the concentration of dopants in the semiconductor material. In the case of BNNS, the carbon concentration also causes a narrow depletion region, allowing electrons to move above its thermal equilibrium value. Since a large amount of carriers are generated in the depletion region, not all valence electron becomes free electrons, so some are trapped by the impurities in the sample, so these are also related to the hysteresis effect.

Au/ BNNS/Mo Schottky barriers are analogous to those of Au/BNNS/Au. However, when interacting with two types of contacts, barrier heights are asymmetric. In other words, their values are not the same. This behavior could be observed from their I–V characteristic curves that would be discussed later.

3.3. Transport properties

Now, we focus on analyzing the electrical properties of BNNS films with two-dimensional features in Au/ BNNS/Au and Au/BNNS/Mo Schottky contacts. Then, we will study the effect of temperature on the current-voltage (I–V) characteristic curve.

BNNSs exhibit very promising electrical properties when a very small amount of current passes through them. Previous experiments have shown that C-doped BNNS could increase the adsorption energy of NO and NO_2 [45], thereby changing its electronic structure and band gap value. This change in settings makes it exhibit stable hysteresis characteristics, especially when analyzing under low voltage levels between terminals. Consequently, BNNS thin film shows a hysterical region close to the origin point when measured on scales from 0 a 3 V in steps of 0.01 V, both in forward and reverse bias voltages, as shown in figures 4(a) and (b). When the temperature changes between 20 and 100 °C, a hysteresis symmetric structure in the range of ± 0.1 to ± 0.2 V can be seen, and high thermal stability is maintained. This makes it a promising candidate for a 2D material with the hysteresis characteristics of two back-to-back connected Schottky junctions. In addition, it is observed that the hysteresis at 100 °C is slightly higher than that at 20 °C, which may be due to the increase in electron tunneling oscillating near that interval and boron vacancies that act as trapping centers. These electrical changes can be seen in detail in the upper part of the I–V illustrations. Many factors will affect the hysteresis effect. Doping content and interface structure may play a dominant role in these phenomena. A high degree of hysteresis stability over a wide range can be achieved in a heavily doped wide-bandgap material where charge trapping is justified and enhanced. This should be important for future memory devices or electronic systems.

A more in-depth study is essential if hysteresis is to be obtained over a wide range of voltage since until now the stability of the Schottky contact with hysteresis at low voltages has been demonstrated. One of the techniques to enhance the electrical properties of BNNS is to decrease the bandgap through doping; in this case, a small amount of carbon was added, which in turn created Boron vacancies, thus converting it into a material with n-type characteristics.

If the operating conditions of Au/BNNS/Au Schottky diodes are taken from 0 to ± 20 V in steps of ± 0.1 V, non-ohmic behavior is dominant, and the hysteresis of BNNS film is negligible at 25 and 100 °C, as shown in figures 4(c) and (d).

Previous studies have shown that charge trap states at the SiO_2/h-BN interface were not sufficiently changed in hysteresis because they were occupied by electron-hole pairs, which suggests the h-BN film is sufficiently thick and prevents electron tunneling, thus creating a clean and inert interface. Through carbon doping, h-BNNS layers show improved conductivity, generating a small amount of free charges on the SiO_2/BNNS interface by the action of a low voltage supply (0 to 3 V in steps of 0.01 V) through Au/BNNS/Au junctions. Conversely, if the voltage increases from 0 to 20 V in steps of 0.1 V, this effect is not appreciated. Therefore, the Schottky barrier potential acts as a high-speed current rectifier at the metal-semiconductor junction, where hysteresis is not appreciable due to its small interaction surface, thereby reducing charge traps in the junctions.

On the other hand, in Au/BNNS/Mo Schottky barrier diodes, hysteresis is dominated at small forward bias voltages taken from 0 to 3 V in steps of 0.01 V, forming various charge traps around 0.09 and 0.17 V, as shown in

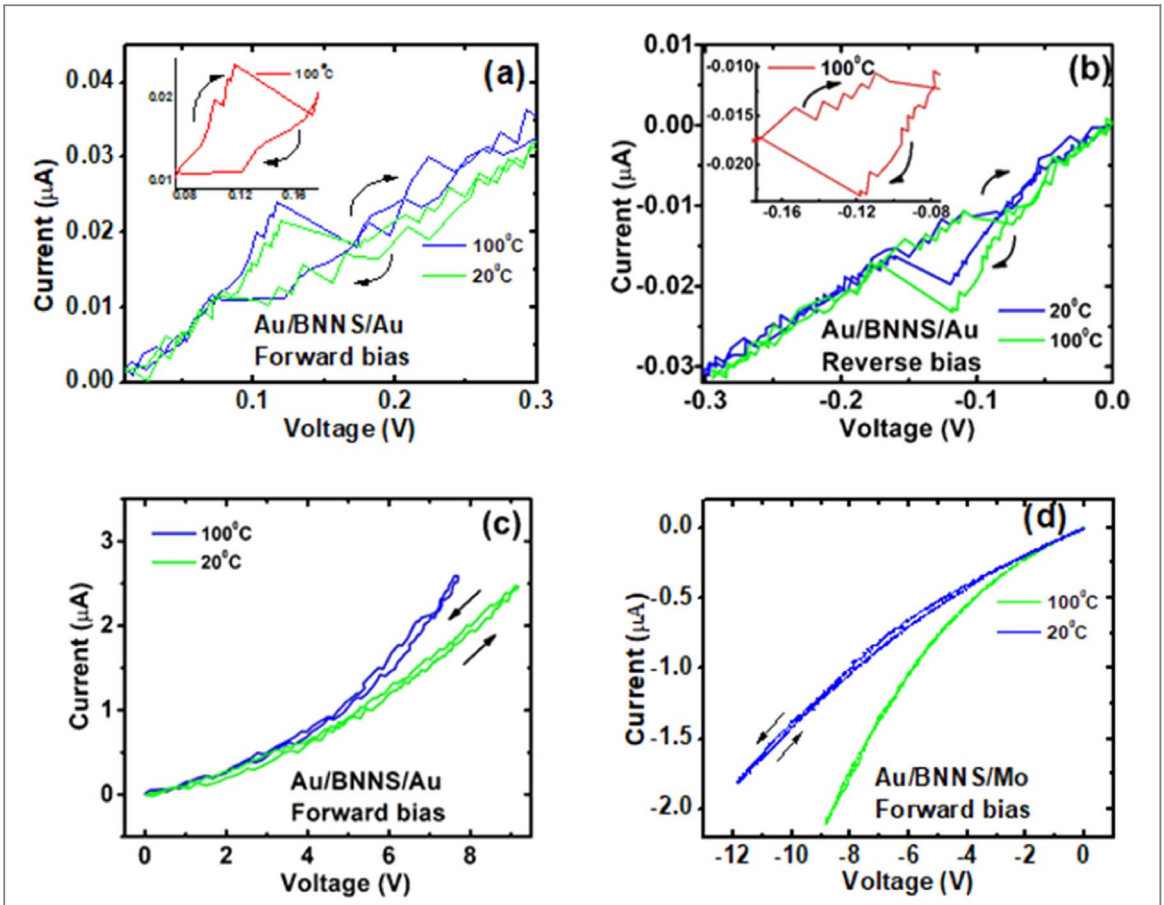

Figure 4. Au/BNNS/Au Schottky contacts with and without hysteresis on Si/SiO_2 substrates taken in 0.01 V and 0.1 V steps at temperatures of 20 °C and 100 °C in the I–V curve. (a) At a low level of forward bias, (b) at a low level of reverse bias, (c) at a high level of forward bias, (d) at a high level of reverse bias.

figure 5(a). The temperature change from 20 to 170 °C is not changed its hysteresis characteristics thus ensuring the maximum stability in high-temperature environments. Instead, under the reverse bias voltage, the hysteresis becomes unstable and the change is not sufficiently visible, which may contradict the analyzed precondition, as shown in figure 5(b). This effect may be due to the change of Schottky barrier height by the junctions of two metals with different work functions and the semiconductor. In addition, the contact area between the junctions is not the same, so an asymmetric curve appears in the I–V curve. The obtained experimental data clearly indicated that the samples are very stable over a wide temperature range. Doping content and the interface structure may be a dominant factor in back-to-back contacts. Differences in symmetry and applied voltages due to the different structures of BNNS/Au or BNNS/Mo suggests that charge traps reduce its mobility at the metal/BNNS interface.

Au/BNNS/Mo Schottky contacts taken from 0 to $\pm$20 V in steps of $\pm$0.1 V has peculiar characteristics in the forward bias region with a higher speed at a higher temperature in the I–V curve, as shown in figure 5(c). Increased tunnel current and the thermal voltage affect the Schottky barrier heights, which depend on the work function of the metal and semiconductor [46, 47]. When characterizing the Au/BNNS/Mo junctions, we observed that the Au/BNNS contact gives faster recombination of the electrons and holes than that of the Molybdenum. These changes allow the behavior of the back-to-back Schottky contact to be asymmetric as discussed above. In addition, charge traps of the majority carriers (electrons) by sample impurities in the bandgap region are considerably reduced by the presence of a large electric field, without the need for so much thermal energy.

As we have seen symmetric and asymmetric contacts, the electron tunneling mechanism and electron emission are universal. Because of the different methods that exist in the transfer of electrons; as for example, Poole-Frenkel emission, Schottky emission, Space-Charge-Limited-Conduction, trap-assisted tunneling, and hopping conduction are attributed to both tunneling and electron emission. However, these effects largely depend on the junction of the material and its characteristic electrical properties. In the case of two-dimensional hexagonal boron nitride nanosheets, this is attributed to electron tunneling at the metal/semiconductor interface and electron emission caused by temperature changes. The novelty of this material is that it can

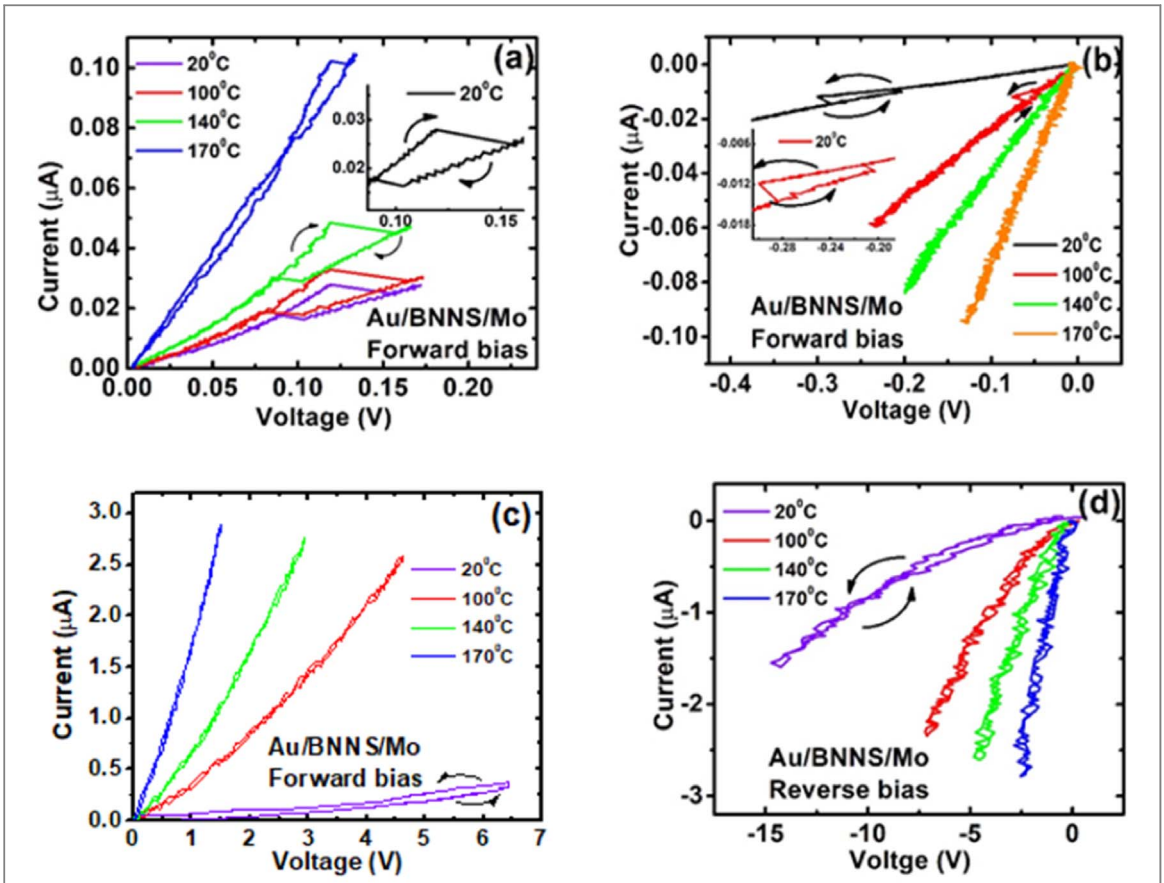

Figure 5. Au/BNNS/Mo Schottky contacts (a)–(b) with and without hysteresis effect taken from 0 to ±3 V in steps of 0.01 V in the I–V curve, (c)–(d) with and without hysteresis effect taken from 0 to ±20 V in steps of 0.1 V.

enhance the device performance and data retention due to its functional properties, thermal-mechanical stability, and its relationship with resistive switching phenomena.

The current-voltage characteristic of a Schottky diode is described by the equation

$$I = I_s\left[\exp\left(\frac{qV_D}{\eta kT}\right) - 1\right], \tag{3}$$

where I_s is the saturation current ($I_s \approx 10^{-12}$ to 10^{-6} A) [48, 49], η is the ideality factor (η typically varies from 1 to 2), k is the Boltzmann constant ($k = 1.38 \times 10^{-23}\,\mathrm{m^2kgs^{-2}K^{-1}}$), T is the absolute temperature, and V_D is the applied voltage. I_s is given by

$$I_s = AA^*T^2e^{-\frac{\Phi_B}{kT}}, \tag{4}$$

where A is the active Schottky diode area ($A_{Au/BNNS/Au} = 3 \times 10^{-11}\mathrm{m^2}$, $A_{Au/BNNS/Mo} = 7.85 \times 10^{-5}\mathrm{m^2}$), A^* is the Richardson constant ($A^* = 3.12 \times 10^5\,\mathrm{Am^{-2}K^{-2}}$), and Φ_B is the barrier height. Just like there are two Schottky contacts connected back-to-back, equations (3) and (4) can be written as two different voltage drops on single diodes, one polarized in the forward and the other in the reverse direction. Since the charge flowing through them are the same, we may express the diode equations with ideality factors [50, 51].

$$I = I_{s1}\left[\exp\left(\frac{qV_{D1}}{\eta kT}\right) - 1\right] Forward, \tag{5}$$

$$I = -I_{s2}\left[\exp\left(-\frac{qV_{D2}}{\eta kT}\right) - 1\right] Reverse, \tag{6}$$

where V_{D1} and V_{D2} are the voltage drops on single diodes. The equations are then

$$V_{D1} = \frac{\eta kT}{q}\ln\left(\frac{I}{I_{s1}} + 1\right), \tag{7}$$

$$V_{D2} = -\frac{\eta kT}{q}\ln\left(-\frac{I}{I_{s1}} + 1\right), \tag{8}$$

and their sum is equal to the external voltage ($V_{D1} + V_{D2} = V$). By performing some mathematical techniques, we can express the current in the form of back-to-back Shottky diodes as

$$I = \frac{2\frac{I_{s1}}{A_1}\frac{I_{s2}}{A_2}\sinh\left(\frac{qV_D}{2\eta kT}\right)}{\frac{I_{s1}}{A_1}\exp\left(-\frac{qV_D}{2\eta kT}\right) + \frac{I_{s2}}{A_2}\exp\left(\frac{qV_D}{2\eta kT}\right)}, \tag{9}$$

where A_1 and A_2 are the contact areas of the single diodes.

The series resistance of the Schottky diode mainly comes from the bulk resistance of the semiconductor, which is the limiting factor for the high voltage operations at the metal/semiconductor junction, i.e., if the current increases, the voltage drop on the series resistance also increases. Therefore, equation (3) can be rewritten as

$$I = I_s\left[\exp\left(\frac{q(V - R_sI)}{\eta kT}\right) - 1\right], \tag{10}$$

where V is the applied voltage, R_s is the semiconductor resistance, I is the electrical current, and $V_D = V - R_sI$ is the back-to-back Schottky diode voltage drop [52, 53].

In actual asymmetric contact, the barrier height on single diodes has different ideality factors. This type of contact cannot be described by a simple analytical equation, it is necessary to write the voltage drop expressions on single diodes with their respective ideality factors y adding the voltage drop on the series resistance

$$V = V_{D1} + V_{D2} + R_sI, \tag{11}$$

$$V_1 = \frac{\eta_1 kT}{q}\ln\left(\frac{I}{I_{s1}} + 1\right), \tag{12}$$

$$V_2 = -\frac{\eta_2 kT}{q}\ln\left(-\frac{I}{I_{s2}} + 1\right). \tag{13}$$

The Schottky barrier plays a central role in lowers the metal work functions, whose values range from 4.6 (molybdenum) to 5.2 eV (gold). The barrier heights of Au/BNNS/Au Schottky diodes range from 0.332 to 0.732 eV in the forward and from 0.326 to 0.723 eV in the reverse. These slight variations do not significantly modify the symmetry of the I–V curve shown in figures 4(c) and (d). Instead, in Au/BNNS/Mo junctions, values range from 0.763 to 1.043 eV in the forward (BNNS/Mo) and from 0.570 to 0.976 eV in the reverse (BNNS/Au). In fact, results show that BNNS / Au junctions reduce Schottky barrier heights better than BNNS/Mo junctions, which also influence the asymmetry of the I–V curve presented in figures 5(c) and (d). Also, when changing the environment conditions from 20 to 170 °C, the barrier heights increase, which may be to the current increase through the metal/semiconductor junction since more electrons have sufficient energy to surmount the higher barrier due to thermal voltage.

On the one hand, in the symmetrical structure, the leakage current decreases slightly with the increase in temperature, both in forward (1.53×10^{-6} to 8.51×10^{-8} A) and reverse bias (1.90×10^{-6} to 1.01×10^{-6} A). This abnormal behavior of the diode indicates that recombination of carriers is affected by thermal voltage as well as trap-assisted tunneling current. Instead, in the asymmetric structure is the opposite both forward (1.57×10^{-7} to 6.38×10^{-6} A) and reverse bias (1.13×10^{-6} to 5.03×10^{-6} A), which is typical of Schottky diodes when the absence of charge is higher in the junctions. This effect is also related to the contact area of the asymmetric junction (3×10^{-11} m^2) is much larger than the symmetric contact (7.85×10^{-5} m^2), which generates larger recombination of electron tunneling through the Schottky contact surface, thereby increasing the leakage current as of the temperature increases.

The parameter that allows specifying the metal-semiconductor junction is the ideality factor η. When Schottky diodes are dominated by ideal thermionic emission the ideality factor η has a range of 1. However, when other physical mechanisms are added to thermionic emissions, such as thermally assisted tunneling and field-enhanced tunneling, η becomes larger than 1. In the back-to-back Schottky diode, the calculation of the ideality factor is based on the mechanism of the voltage drop across the individual barriers. The values obtained in Au/BNNS/Au contacts are in the forward range from 2.50 to 1.22 and in the reverse range from 4.38 to 1.66. In this procedure, we observed that η decreases with increasing temperature from 20 to 100 °C. Likewise, in Au / BNNS / Mo contacts, η is in the range from 1.79 to 1.04 in the forward, and from 4.16 to 1.83 in the reverse, which is similar to the previous case, but this time the conditions were from 20 to 170 °C. This indicates that diffusion currents are increased due to the thermionic effect, and the thermal energy provided to the charge carriers is larger than the work function of the conductor material.

Since electrons pass through the BNNS film at a low energy level than the Schottky barrier height, the tunneling effect affects the hysteresis characteristics of the material. Solving the Schrodinger equation in one dimension allows us to understand these physical details through the transmission coefficient, which is proportional between the modules of the square wave function as

$$T = \frac{|\Psi_B|^2}{|\Psi_A|^2} = \left[1 + \frac{{U_0}^2 \sin h^2(|k|\ d)}{4E(U_0 - E)}\right]^{-1}, \tag{14}$$

$$T \sim \exp\left(-2\sqrt{\frac{2m(E - U_0)}{\hbar^2}}\, d\right), \tag{15}$$

where Ψ_A is the wave function in the conductor region, Ψ_B in the semiconductor, U_0 is the barrier potential ($U_0 = \Phi_B$), d is the width (film thickness), E is the energy of the electron ($E < U_0$), m is the mass of the electron, and $k = \sqrt{\frac{2m(E - U_0)}{\hbar}}$. When the depletion zone is about 10 nm or less, it promotes electron tunneling, which is conducive to charge flow and reduces hysteresis. Since the thickness of BNNS is around 3–4 nm, the tunneling effect would affect the hysteresis characteristics, leading to a lowering of the energy barrier due to the interaction with the electric field in the metal-semiconductor interface.

4. Conclusions

Au/BNNS/Au Schottky contacts favor the reduction of the tunneling effects and carrier recombination, maintaining an almost constant flow of electrons through the BNNSs film. Under low bias voltage, it exhibits a stable symmetric hysteresis and improved adsorption energy by the concentration of a slight amount of carbon in the BNNS two-dimensional atomic layers.

On the other hand, Au/BNNS/Mo Schottky barrier exhibits stable hysteresis characteristics under low bias voltages in environments up to 170 °C. When electrons tunnel from the Mo-BNNS to the BNNS-Au interface, the hysteresis effect is reduced in the sequential I–V seeping. This suggests that in reverse bias there is little effect on the emission of the electron traps due to the action of a large electrical field at the junction, which is compatible with the Poole-Frenkel effect. When the charge switching speed increases rapidly with a slight increase in bias voltage and temperature, the hysteresis area becomes smaller and smaller, which makes it a rectifier with low energy loss.

It can be concluded that the hysteresis loops in Au/BNNS/Au and Au/BNNS/Mo Schottky diodes are directly affected by variable parameters of series resistance and barrier lowering. The mechanism of the charge traps could be attributed to the electrons directly tunneling on the interface, and the release of trapped electrons due to thermionic emission. This is convincing with observations made at the Schottky barrier when current-voltage (I–V) operating conditions change at the BNNS film.

Acknowledgments

This work is financially supported by NSF-CREST Center for Innovation, Research and Education in Environmental Nanotechnology (CIRE2N) Grant Number HRD-1736093. University of Puerto Rico Molecular Science Research building (MSRB) offers specialized services with research equipment.

Data availability statement

All data that support the findings of this study are included within the article (and any supplementary files).

ORCID iDs

Wilber Ortiz https://orcid.org/0000-0002-8609-7194
Mohan K Bhattarai https://orcid.org/0000-0002-8227-4827

References

[1] Jeevanandam J, Barhoum A, Chan Y S, Dufresne A and Danquah M K 2018 Review on nanoparticles and nanostructured materials: history, sources, toxicity and regulations *Beilstein J. Nanotechnol.* **9** 1050–74
[2] Li L H, Cervenka J, Watanabe K, Taniguchi T and Chen Y 2014 Strong oxidation resistance of atomically thin boron nitride nanosheets *ACS Nano* **8** 1457–62
[3] Berseneva N, Gulans A, Krasheninnikov A V and Nieminen R M 2013 Electronic structure of boron nitride sheets doped with carbon from first-principles calculations *Physical Review B* **87** 035404

[4] Park H, Wadehra A, Wilkins J W and Castro Neto A H 2012 Magnetic states and optical properties of single-layer carbon-doped hexagonal boron nitride *Appl. Phys. Lett.* **100** 253115–4
[5] Zhao J and Chen Z 2015 Carbon-doped boron nitride nanosheet: an efficient metal-free electrocatalyst for the oxygen reduction reaction *J. Phys. Chem. C* **119** 26348–54
[6] Zhao C, Xu Z, Wang H, Wei J, Wang W, Bai X and Wang E 2014 Carbon-doped boron nitride nanosheets with ferromagnetism above room temperature *Adv. Funct. Mater.* **24** 5985–92
[7] Esrafili M D and Saeidi N 2018 Carbon-doped boron nitride nanosheet as a promising catalyst for N_2O reduction by CO or SO_2 molecule: a comparative DFT study *Appl. Surf. Sci.* **444** 584–9
[8] Huang C, Chen C, Zhang M, Lin L, Ye X, Lin S, Antonietti M and Wang X 2015 Carbon-doped BN nanosheets for metal-free photoredox catalysis *Nat. Commun.* **6** 1–7
[9] Guerra V, Wan C and McNally T 2019 Thermal conductivity of 2D nano-structured boron nitride (BN) and its composites with polymers *Prog. Mater. Sci.* **100** 170–86
[10] Wang X, Pakdel A, Zhi C, Watanabe K, Sekiguchi T, Golberg D and Bando Y 2012 High-yield boron nitride nanosheets from 'chemical blowing': towards practical applications in polymer composites *J. Phys.: Condens. Matter* **24** 314205
[11] Min Y J, Kang K H and Kim D E 2018 Development of polyimide films reinforced with boron nitride and boron nitride nanosheets for transparent flexible device applications *Nano Res.* **11** 2366–78
[12] Teng C, Su L, Chen J and Wang J 2019 Flexible, thermally conductive layered composite films from massively exfoliated boron nitride nanosheets *Compos. Part A Appl. Sci. Manuf.* **124** 105498
[13] Zou X *et al* 2016 Dielectric engineering of a boron nitride/hafnium oxide heterostructure for high-performance 2D field effect transistors *Adv. Mater.* **28** 2062–9
[14] Zhang K, Feng Y, Wang F, Yang Z and Wang J 2017 Two dimensional hexagonal boron nitride (2D-hBN): synthesis, properties and applications *J. Mater. Chem. C* **5** 11992–2022
[15] Wirtz L, Marini A and Rubio A 2005 Optical absorption of hexagonal boron nitride and BN nanotubes *AIP Conf. Proc.* **786** 391–5
[16] Basu R and Atwood L J 2019 Two-dimensional hexagonal boron nitride nanosheet as the planar-alignment agent in a liquid crystal-based electro-optic device *Opt. Express* **27** 282
[17] Slaoui A, Fogarassy E, Fuchs C and Siffert P 1992 Properties of silicon dioxide films prepared by pulsed-laser ablation *J. Appl. Phys.* **71** 590–6
[18] Smit G D J, Rogge S and Klapwijk T M 2002 Scaling of nano-Schottky-diodes *Appl. Phys. Lett.* **81** 3852–4
[19] Rezeq M, Eledlebi K, Ismail M, Dey R K and Cui B 2016 Theoretical and experimental investigations of nano-Schottky contacts *J. Appl. Phys.* **120** 044302
[20] Zhao H *et al* 2017 Atomically thin femtojoule memristive device *Adv. Mater.* **29** 1703232–7
[21] Choi G, Yoon H H, Jung S, Jeon Y, Lee J Y, Bahng W and Park K 2015 Schottky barrier modulation of metal/4H-SiC junction with thin interface spacer driven by surface polarization charge on 4H-SiC substrate *Appl. Phys. Lett.* **107** 252101–5
[22] Yuan H, Song Q W, Han C, Tang X Y, He X N, Zhang Y M and Zhang Y M 2019 Hysteresis effect in current-voltage characteristics of Ni/n-type 4H-SiC Schottky structure *Chin. Phys. B* **28** 117303–117303
[23] Wu X, Ge R, Chen P A, Chou H, Zhang Z, Zhang Y, Banerjee S, Chiang M H, Lee J C and Akinwande D 2019 Thinnest nonvolatile memory based on monolayer h-BN *Adv. Mater.* **31** 1806790–7
[24] Sanchez Esqueda I, Zhao H and Wang H 2018 Efficient learning and crossbar operations with atomically-thin 2-D material compound synapses *J. Appl. Phys.* **124** 152133–5
[25] Zhi Y S, Li P G, Wang P C, Guo D Y, An Y H, Wu Z P, Chu X L, Shen J Q, Tang W H and Li C R 2016 Reversible transition between bipolar and unipolar resistive switching in Cu_2O/Ga_2O_3 binary oxide stacked layer *AIP Adv.* **6** 015215–7
[26] Jeong D S and Hwang C S 2005 Tunneling-assisted Poole-Frenkel conduction mechanism in Hf O2 thin films *J. Appl. Phys.* **98** 113701-6
[27] Yeargan J R and Taylor H L 1968 The Poole-Frenkel effect with compensation present *J. Appl. Phys.* **39** 5600–4
[28] Hanna M J, Zhao H and Lee J C 2012 Poole Frenkel current and Schottky emission in SiN gate dielectric in AlGaN/GaN metal insulator semiconductor heterostructure field effect transistors *Appl. Phys. Lett.* **101** 153504–4
[29] Xiong C, Lu Z, Yin S, Mou H and Zhang X 2019 Magnetic field controlled hybrid semiconductor and resistive switching device for non-volatile memory applications *AIP Adv.* **9** 105030–6
[30] Li T, Du G, Zhang B and Zeng Z 2014 Scaling behavior of hysteresis in multilayer MoS2field effect transistors *Appl. Phys. Lett.* **105** 093107–5
[31] Kaushik N, Mackenzie D M A, Thakar K, Goyal N, Mukherjee B, Boggild P, Petersen D H and Lodha S 2017 Reversible hysteresis inversion in MoS_2 field effect transistors npj 2D *Materials and Applications* **1** 34–9
[32] Sajjad M, Peng X, Chu J, Zhang H and Feng P 2013 Design and installation of a CO_2 -pulsed laser plasma deposition system fo. The growth of mass product nanostructures *J. Mater. Res.* **28** 1747–52
[33] Cai Q, Scullion D, Falin A, Watanabe K, Taniguchi T, Chen Y, Santos E J G and Li L H 2017 Raman signature and phonon dispersion of atomically thin boron nitride *Nanoscale* **9** 3059–67
[34] Wan S, Yu Y, Pu J and Lu Z 2015 Facile fabrication of boron nitride nanosheets-amorphous carbon hybrid film for optoelectronic applications *RSC Adv.* **5** 19236–40
[35] Ahmad P *et al* 2019 Fabrication of hexagonal boron nitride quantum dots via a facile bottom-up technique *Ceram. Int.* **45** 22765–8
[36] Falin A *et al* 2017 Mechanical properties of atomically thin boron nitride and the role of interlayer interactions *Nat. Commun.* **8** 15815
[37] Li L H and Chen Y 2016 Atomically thin boron nitride: unique properties and applications *Adv. Funct. Mater.* **26** 2594–608
[38] Chubarov M, Högberg H, Henry A and Pedersen H 2018 Review article: challenge in determining the crystal structure of epitaxial 0001 oriented sp 2 -BN films *Journal of Vacuum Science & Technology A: Vacuum, Surfaces, and Films* **36** 030801
[39] Guerra V, Wan C, Degirmenci V, Sloan J, Presvytis D and McNally T 2018 2D boron nitride nanosheets (BNNS) prepared by high-pressure homogenisation: structure and morphology *Nanoscale* **10** 19469–77
[40] Maghsoudy-Louyeh S, Kropf M and Tittmann B R 2019 Review of progress in atomic force microscopy *The Open Neuroimaging Journal* **12** 86–104
[41] Li Y, Garnier V, Steyer P, Journet C and Bérangè Re Toury B 2020 Millimeter-scale hexagonal boron nitride single crystals for nanosheet generation*ACS Appl. Nano Mater.* **3** 1508–15
[42] Esrafili M D and Arjomandi Rad F 2019 Carbon-doped boron nitride nanosheets as highly sensitive materials for detection of toxic NO and NO_2 gases: a DFT study *Vacuum* **166** 127–34
[43] Feng P X and Sajjad M 2012 Few-atomic-layer boron nitride sheets syntheses and applications for semiconductor diodes *Mater. Lett.* **89** 206–8

[44] Sajjad M, Ahmadi M, Guinel M J F, Lin Y and Feng P 2013 Large scale synthesis of single-crystal and polycrystalline boron nitride nanosheets *J. Mater. Sci.* **48** 2543–9
[45] Dökme I 2011 The analysis of I–V characteristics of Schottky diodes by thermionic emission with a Gaussian distribution of barrier height *Microelectron. Reliab.* **51** 360–4
[46] Latreche A 2019 Combined thermionic emission and tunneling mechanisms for the analysis of the leakage current for Ga_2O_3 Schottky barrier diodes *SN Applied Sciences* **1** 188–9
[47] Yuan Z, Nainani A, Sun Y, Lin J-Y J, Pianetta P and Saraswat K C 2011 Schottky barrier height reduction for metal/n-GaSb contact by inserting TiO_2 interfacial layer with low tunneling resistance *Appl. Phys. Lett.* **98** 172106
[48] Sklyarchuk V M, Gnatyuk V A, Pylypko V G and Aoki T 2020 Schottky diode detectors with low leakage current at high operating voltage *Lecture Notes in Networks and Systems* 101 (Berlin: Springer) pp 159–67
[49] Peta K R and Kim M D 2018 Leakage current transport mechanism under reverse bias in Au/Ni/GaN Schottky barrier diode *Superlattices Microstruct.* **113** 678–83
[50] Osvald J 2015 Back-to-back connected asymmetric Schottky diodes with series resistance as a single diode *Phys. Status Solidi* **212** 2754–8
[51] Nouchi R 2014 Extraction of the Schottky parameters in metal-semiconductor-metal diodes from a single current-voltage measurement *J. Appl. Phys.* **116** 184505
[52] Lien C D, So F C T and Nicolet M A 1984 An Improved forward I–V method for nonideal Schottky diodes with high series resistance *IEEE Trans. Electron Devices* **31** 1502–3
[53] Cheung S K and Cheung N W 1986 Extraction of Schottky diode parameters from forward current-voltage characteristics *Appl. Phys. Lett.* **49** 85–7